2015-2019326

SciTech 2015, 5–9 January 2015, Kissimmee, FL

Discontinuous High-Order Finite-Volume/Finite-Element Method for Inviscid Compressible Flows

Ali Ramezani*, Goran Stipcich*, Lakhdar Remaki†

BCAM - Basque Center for Applied Mathematics, Mazarredo 14, E48009 Bilbao, Basque Country, Spain

The discontinuous, hybrid control-volume/finite-element method merges the desirable conservative properties and intuitive physical formulation of the finite-volume technique, with the capability of local arbitrary high-order accuracy distinctive of the discontinuous finite-element method. This relatively novel scheme has been previously applied to the solution of advection-diffusion problems and the shallow-water equations, and is in the present work extended to the Euler equations. The derivation of the method is presented in the general multi-dimensional case, and selected numerical problems are solved in the one- and two-dimensional case.

Nomenclature

$\mathbf{A}$	Flux Jacobian matrix
$\mathbf{f}$	Flux quantities vector
$\mathbf{n}$	Unit normal vector
$\mathbf{u}$	State variables vector
$\mathbf{x}$	Position vector, m
d	Spatial dimension of the problem
E	Total energy per unit volume, $\mathrm{N/m^2}$
e	Element
h	Mesh size
L	Lagrange polynomials
p	Pressure, $\mathrm{N/m^2}$
P^e	Elemental polynomial order
t	Time, s
u, v	Cartesian velocity components, m/s
V	Control volume

Subscripts

i, j	Running indices

Symbols

$\widetilde{\mathbf{u}}$	Limited state variables vector
$\widehat{\mathbf{f}}$	Numerical flux vector
Ω	Computational domain
ϕ	Test function
ρ	Density, $\mathrm{kg/m^3}$
$\mathcal{T}_h$	Discretization of the domain

*Researcher, BCAM - Basque Center for Applied Mathematics, Mazarredo 14, E48009 Bilbao, Spain.

†Professor, BCAM - Basque Center for Applied Mathematics, Mazarredo 14, E48009 Bilbao, Spain.

$\bar{\cdot}$ Closure of a set in $\mathbb{R}^d$

Superscripts

$-$, $+$ One-sided limit solution

I. Introduction

THE hybrid finite-volume/finite-element method (CVFEM) arises from the instance of merging the excellent numerical conservation properties and the intuitive physical formulation distinctive of the finite-volume methodology, with the geometrical flexibility of the finite-element method, resulting in the vertex- or node-based finite-volume method. The CVFEM can be seen as a finite-element method in which volume indicator distributions are used as weight functions.[1] The method has been developed originally by[2] for advection-diffusion problems on triangular elements, where the integral conservation equations are enforced on polygonal control volumes constructed around each node of the mesh. The CVFEM has been further extended to incompressible flow using bilinear, quadrilateral elements and tetrahedral elements.[3,4,5,6] A detailed analysis of consistent and lumped versions of the CVFEM algorithm for diffusion-type problems has been carried out.[7] Some of the positive characteristics of the CVFEM approach are pointed out: local conservation is achieved at control volume level and the discrete maximum principle[8] is preserved. A high-order CVFEM for unstructured grids was proposed by[9] for advection-diffusion problems, featuring a quadrature-free approach on quadrilateral elements. It is shown that an appropriate distribution of interpolation points and control-volume edges leads to a well conditioned matrix.

Discontinuous methods have been developed at first in the finite-element framework. The resulting discontinuous Galerkin methods (DG), are characterized by the relaxation of the continuity constraint between neighboring elements, which is imposed in weak form through the *numerical fluxes*.[10,11] The specific formulation of numerical fluxes strongly affects the consistency, stability and accuracy of the method.[10] The discontinuous philosophy has been applied within the CVFEM framework,[12,13] giving rise to discontinuous control volume/finite element methods (DCVFEM, hereafter). Research in this area has been mainly focused on hyperbolic problems.[12,13] The continuous Galerkin finite-element method, Taylor-Galerkin Least Square finite elements, DG and DCVFEM are compared in[13] for the solution of the linear advection equation, using quadrilateral elements with interpolating polynomials of degree four to nine. The spatial discretization comprises a *dual* grid structure, the globally elemental unstructured subdivision and the local structured control-volume subdivision. The authors remark the straightforward ability to implement slope or flux limiters inherent in the DCVFEM formulation.[13] The DCVFEM has been applied to the solution of the advection-diffusion equation in the one- and two-dimensional case.[14] A formal derivation is provided, along with a detailed Fourier analysis, and the spectral accuracy of the method is verified by theoretical and numerical results.

The present work, the DCVFEM is extended to the solution of the Euler equations in the one- and two-dimensional case. The derivation in the general multi-dimensional case is presented, and the method is applied to the solution of selected numerical problems.

II. Model

II.A. Governing equations

The hyperbolic system of conservation laws is considered

$$\partial_t \mathbf{u} + \nabla \cdot \mathbf{f}(\mathbf{u}) = \mathbf{0}, \qquad \mathbf{u}(\mathbf{x}, t) \in \mathbb{R}^n \tag{1}$$

defined on a domain $\Omega \subset \mathbb{R}^d$ with a piecewise smooth boundary $\partial\Omega$. The time partial derivative is denoted as $\partial_t = \partial/\partial t$, $\mathbf{u} = (u_1, \ldots, u_n)^T$ stays for the state variables vector, $\mathbf{x}$ is the spatial coordinate vector, and

$$\mathbf{f} = (\mathbf{f}_1, \ldots, \mathbf{f}_d) : \mathbb{R}^n \longrightarrow (\mathbb{R}^n)^d$$

is a nonlinear mapping with $\mathbf{f}_i : \mathbb{R}^n \longrightarrow \mathbb{R}^n$, $i = 1, \ldots, d$, such that the Jacobian matrix $\mathbf{A} = \partial\mathbf{f}/\partial\mathbf{u}$ have only real eigenvalues.[15] System (1) is closed by the ideal gas law[16] and complemented by suitable initial and boundary conditions.

II.B. Weak formulation

Considering a discretization $\mathcal{T}_h$ of $\overline{\Omega}$ into elements e [17, ch. 3.1], the *discontinuous* approximate solution can be defined by a weighted residual statement.[10] System (1) is multiplied by a weight function ϕ and integrated over the whole domain, and, upon integration by parts, the equation for the single element e read as

$$\int_e \frac{\partial \mathbf{u}}{\partial t}\,\phi\,\mathrm{d}\mathbf{x} - \int_e \mathbf{f}\cdot\nabla\phi\,\mathrm{d}\mathbf{x} + \int_{\partial e} \mathbf{f}\cdot\mathbf{n}\phi\,\mathrm{d}s = \mathbf{0} \tag{2}$$

where $\mathbf{n}$ denotes the outward-pointing normal unit vector. Each element $e \in \mathcal{T}_h$ is further subdivided into control volumes $V \subset e$[13] (see Section II.D), and the weight function ϕ in (2) is chosen to be the volume indicator distribution,[1] defined as

$$\phi \equiv \phi_V(\mathbf{x}) = \begin{cases} 1 & \text{if } \mathbf{x} \in \mathrm{V} \\ 0 & \text{otherwise} \end{cases} \tag{3}$$

System (2) then yields the following weak formulation for the single control volume V

$$\int_V \frac{\partial \mathbf{u}}{\partial t}\,\mathrm{d}\mathbf{x} + \int_{\partial V} \mathbf{f}\cdot\mathbf{n}\,\mathrm{d}s = \mathbf{0} \tag{4}$$

II.C. Coupling conditions: numerical flux

On the boundary of the control volume V, a suitable *numerical flux* $\widehat{\mathbf{f}}$ is defined. The surface integral in (4) is calculated as

$$\int_{\partial V} \mathbf{f}\cdot\mathbf{n}\,\mathrm{d}s \simeq \int_{\partial V} \widehat{\mathbf{f}}\cdot\mathbf{n}\,\mathrm{d}s \tag{5}$$

The definition of the numerical flux is crucial, since it affects the consistency, stability and accuracy of the resulting discontinuous method.[10] In the present work, the Roe's scheme is enforced.[15] In order to avoid detrimental numerical oscillations near shock waves and discontinuities, a slope limiting strategy is applied on the state variables vector. Considering the i-th control volume V, a *local* projection limiting[18] is implemented *componentwisely* as

$$\widetilde{\mathbf{u}}_i^- \simeq \mathbf{u}_i^* + \mathrm{minmod}\left(\mathbf{u}_i^- - \mathbf{u}_i^*,\, \Delta_{i+1}\mathbf{u}^*,\, \Delta_i\mathbf{u}^*\right) \tag{6a}$$

$$\widetilde{\mathbf{u}}_i^+ \simeq \mathbf{u}_i^* - \mathrm{minmod}\left(\mathbf{u}_i^* - \mathbf{u}_i^+,\, \Delta_{i+1}\mathbf{u}^*,\, \Delta_i\mathbf{u}^*\right) \tag{6b}$$

where $\widetilde{\mathbf{u}}$ is the modified state vector, the symbol "$*$" indicates the mean value over the control volume V, and the "$+$" and "$-$" signs denote the one-sided limit solution when approaching the control volume's boundary ∂V. The jumps of the mean values between neighbouring control volumes in a *structured* pattern are given as $\Delta_{i+1}\mathbf{u}^* = \mathbf{u}_{i+1}^* - \mathbf{u}_i^*$ and $\Delta_i\mathbf{u}^* = \mathbf{u}_i^* - \mathbf{u}_{i-1}^*$.[18]

II.D. Space discretization: subdivision into control volumes

Each element $e \in \mathcal{T}_h$ is further subdivided into control volumes, entirely contained in the respective element, accordingly to the local polynomial order of accuracy P^e

$$V_i \subset e, \qquad i = 1, \ldots, (P^e + 1)^d$$

The elemental subdivision forms a *structured* dual partition with respect to the original discretization $\mathcal{T}_h$, allowing for the straightforward implementation of flux schemes and slope limiters on the control volume's boundaries[13] (Section II.C).

In principle, any subdivision into control volumes V can be formed, and in the present work the equally spaced partition is chosen. Figure 1 shows the proposed subdivision for the one- and two-dimensional element, for polynomial orders $P^e = 1, 2$. For $d = 2, 3$, the tensor product of the one-dimensional element is used, as shown in Figure 1(c-d). The mentioned partitioning procedure is naturally extended to any polynomial order P^e.

The DCVFEM features the property, inherent in the discontinuous formulation, that the resulting approximate solution is not required to satisfy any inter-element continuity constrain.[10] As a consequence, different orders of approximation P^e can be employed in different sub-domains of Ω, rendering the method ideal for use with p-adaptivity.[19]

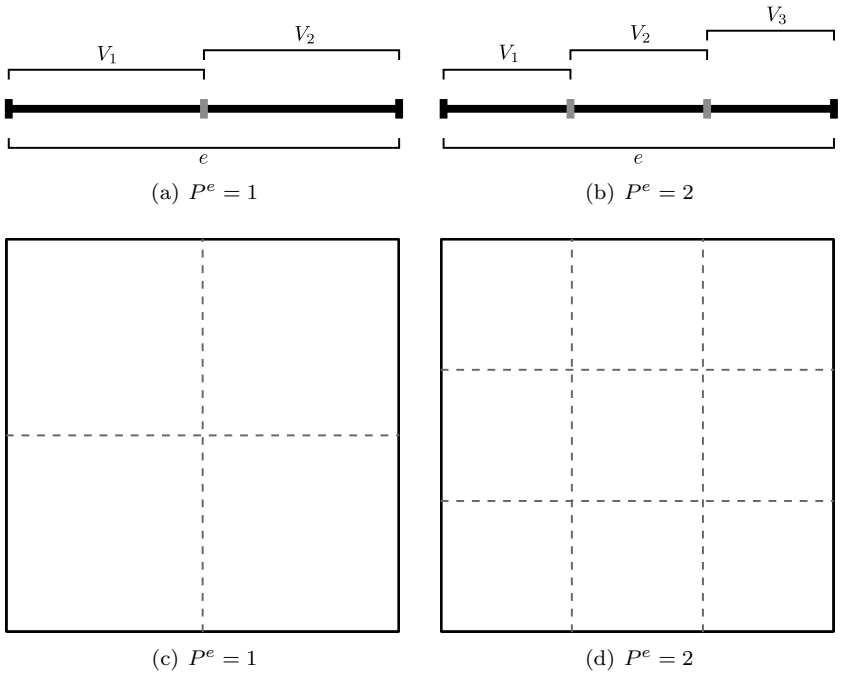

Figure 1. Sketch of the subdivision into control volumes V for a (a-b) one- and (c-d) two-dimensional element e, of polynomial order (left) $P^e = 1$ and (right) $P^e = 2$.

II.E. Finite dimensional subspace and basis functions

The unknowns $\mathbf{u}(\mathbf{x}, t)$ are approximated by element-based polynomial expansions.[11] The numerical approximations $\mathbf{u}_h(\mathbf{x}, t)$ are chosen in the same finite-dimensional subspace of $\mathbb{L}^2(\Omega)$,[17] spanned by a basis of piecewise polynomials L_j, defined in the transformed reference space $[-1, 1]^d$, which do not respect inter-element continuity. In the present work, the Lagrange coefficients are used. For example, the restriction $\mathbf{u}_h^e$ of $\mathbf{u}_h$ to the element e is given by

$$\mathbf{u}_h^e \equiv \sum_j L_j \, \mathbf{u}_j^e, \qquad j = 1, \ldots, (P^e + 1)^d \tag{7}$$

where $\{\mathbf{u}_k^e\}$ is the set of nodal values of $\mathbf{u}_h$ in the element e. In principle, the interpolation nodes may be located everywhere inside an element, and in the present study the equally spaced placement is chosen.

III. Results

System (1), coupled with suitable initial and boundary conditions for selected one- and two-dimensional test cases, is solved using the DCVFEM, and the results are presented in the following. In all the numerical experiments, a fourth order Runge-Kutta quadrature scheme is employed for the time marching.

III.A. One-dimensional case

System (1) is considered in the one-dimensional case ($d = 1$ and $n = 3$):

$$\frac{\partial \mathbf{u}}{\partial t} + \frac{\partial \mathbf{f}}{\partial x} = 0 \tag{8a}$$

$$\mathbf{u} = (\rho, \, \rho u, \, E)^T \tag{8b}$$

$$\mathbf{f} = \left(\rho u, \, \rho u^2 + p, \, u\,(E + p)\right)^T \tag{8c}$$

where ρ denotes the density, u the velocity, p is the pressure and E is the total energy per unit volume.[16] The reference solution is obtained by the finite-volume scheme on a very fine mesh of 10 000 elements, labelled

as "Ref" in the legend.

III.A.1. Sod's shock-tube problem

The shock-capturing capability of the DCVFEM is tested by the Sod shock-tube problem.[20] System (8) is coupled with the following initial conditions

$$(\rho,\, u,\, p) = \begin{cases} (1,\, 0,\, 1) & t = 0,\; x \leq 0.5 \\ (0.125,\, 0,\, 0.1) & t = 0,\; x > 0.5 \end{cases} \tag{9}$$

on the domain $\Omega = [0,\, 1]$. The density distribution is shown in Figure 2 for different polynomial orders of accuracy $P^e = 1,\, 2,\, 3$. A coarse mesh of 100 elements is used.

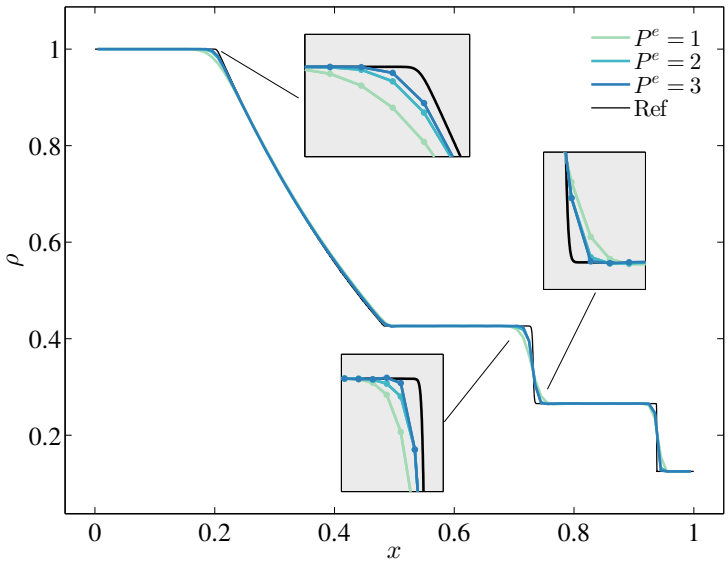

Figure 2. Density distribution for the shock-tube problem (9) on a coarse mesh of 100 elements for $P^e = 1$ to $P^e = 3$. The dots represent the average values over elements.

The following considerations can be made:

- The DCVFEM exhibits a "sharper" shock-capturing as the polynomial order is increased.
- The approximated solution is free from apparent numerical oscillations and overshooting for the considered polynomial orders P^e.

III.A.2. Shu-Osher wave interaction problem

The shock-entropy wave interaction problem[21] is solved in order to test the proposed method on shock-capturing and shock-turbulence interaction. The entropy waves are very sensitive to numerical dissipation introduced by a numerical scheme, and can be excessively damped. Equations (8) are solved, coupled with the following initial condition

$$(\rho,\, u,\, p) = \begin{cases} (3.857143,\, 2.629369,\, 10.33333) & t = 0,\; x < -4 \\ (1 + 0.2\sin(5x), 0, 1) & t = 0,\; x \geq -4 \end{cases} \tag{10}$$

on the domain $\Omega = [-5,\, 5]$. The density distribution is shown in Figure 3 for different polynomial orders of accuracy $P^e = 1,\, 2,\, 3$. A coarse mesh of 200 elements is used.

The following considerations can be made:

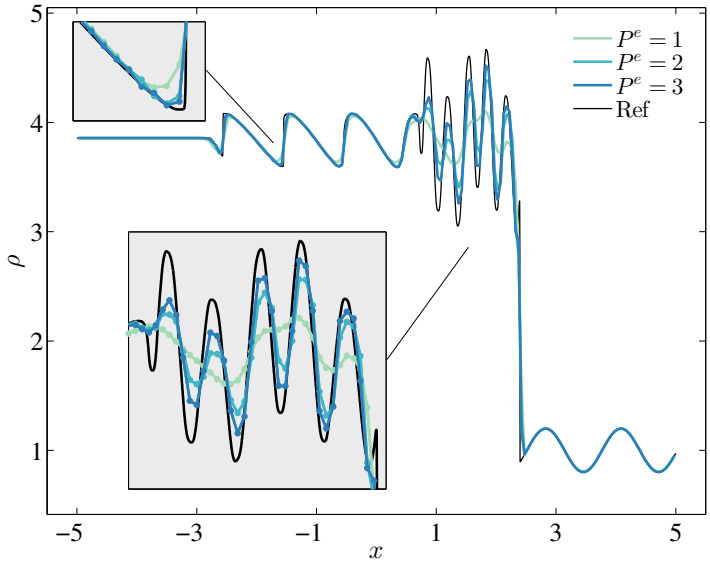

Figure 3. Density distribution for the shock-entropy wave interaction problem (10) on a coarse mesh of 200 elements for $P^e = 1$ to $P^e = 3$. The dots represent the average values over elements.

- The DCVFEM capability of capturing both shocks and small length scales enhances as the polynomial order P^e is increased.
- The approximated solution is free from apparent numerical oscillations and overshooting for the considered polynomial orders P^e.

III.B. Two-dimensional case

Considering the two-dimensional case ($d = 2$ and $n = 4$), system (1) read as

$$\frac{\partial \mathbf{u}}{\partial t} + \frac{\partial \mathbf{f}_1}{\partial x} + \frac{\partial \mathbf{f}_2}{\partial y} = 0 \tag{11a}$$

$$\mathbf{u} = (\rho,\, \rho u, \rho v,\, E)^T \tag{11b}$$

$$\mathbf{f}_1 = \left(\rho u,\, \rho u^2 + p,\, \rho uv,\, u\,(E+p)\right)^T \tag{11c}$$

$$\mathbf{f}_2 = \left(\rho v,\, \rho uv,\, \rho v^2 + p,\, v\,(E+p)\right)^T \tag{11d}$$

where the cartesian components of the velocity are denoted by u, v.

III.B.1. Oblique shock reflection

The oblique shock reflection over an inviscid wall [16, ch. 4] is solved by the DCVFEM on the domain $\Omega = [0,\, 2] \times [0,\, 1]$. A shock with angle of 35.24° is imposed, with a Mach 2 free-stream inflow.

Figure 4 shows the contour of the density ρ, for the DCVFEM solution on a mesh of 80×40 elements for different polynomial orders of accuracy $P^e = 1,\, 2,\, 3$. Equally spaced density contours are plotted for reference. Additionally, a line plot of the density distribution at $y = 0.2$ is shown in Figure 5. The DCVFEM results are compared with the exact solution [16, ch. 4], labelled as "Exact" in the legend. The following considerations can be made:

- A "sharper" shock-capturing capability is achieved by increasing the polynomial accuracy P^e.
- The approximated solution is free from apparent numerical oscillations and overshooting for the considered orders P^e.

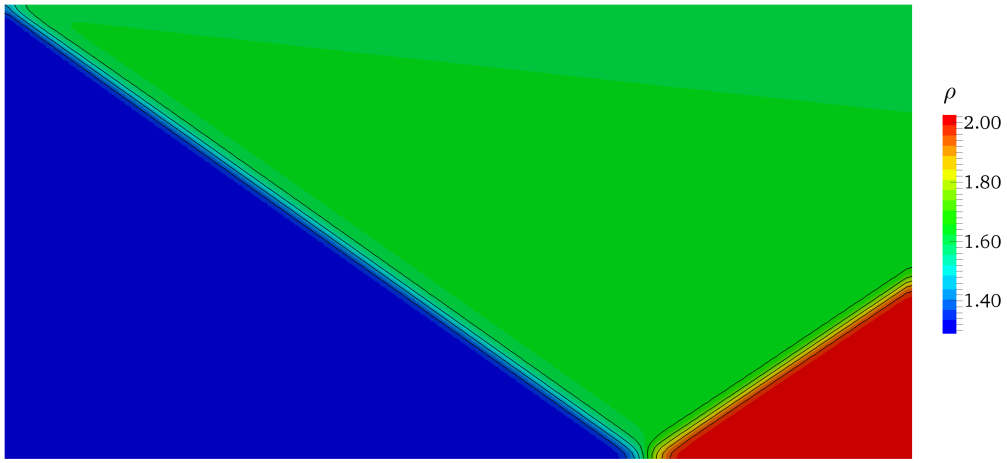

(a) $P^e = 1$

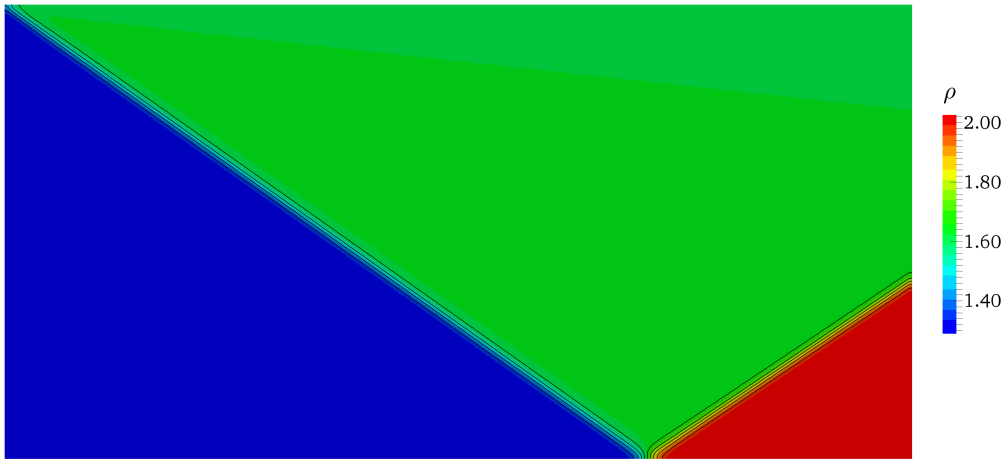

(b) $P^e = 2$

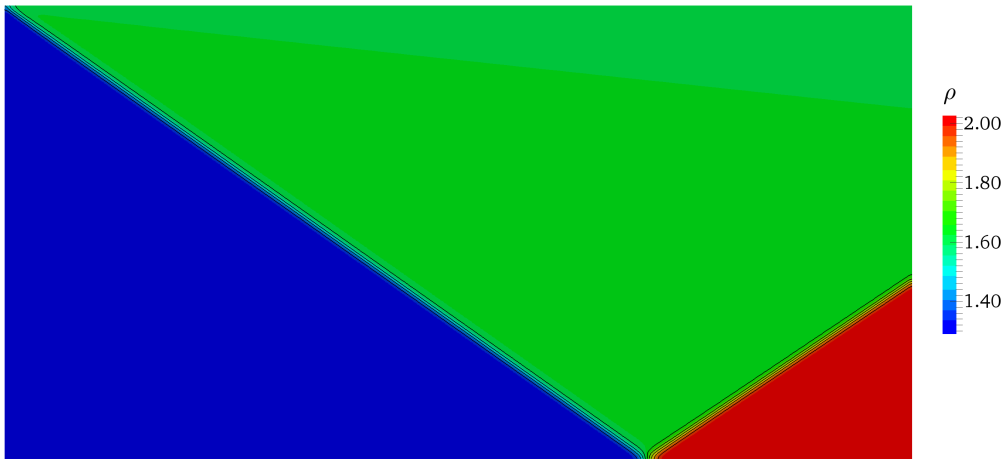

(c) $P^e = 3$

Figure 4. Density distribution for the oblique shock reflection problem on a mesh of 80×40 elements for (a-c) $P^e = 1$ to $P^e = 3$. Equally spaced density contours are shown.

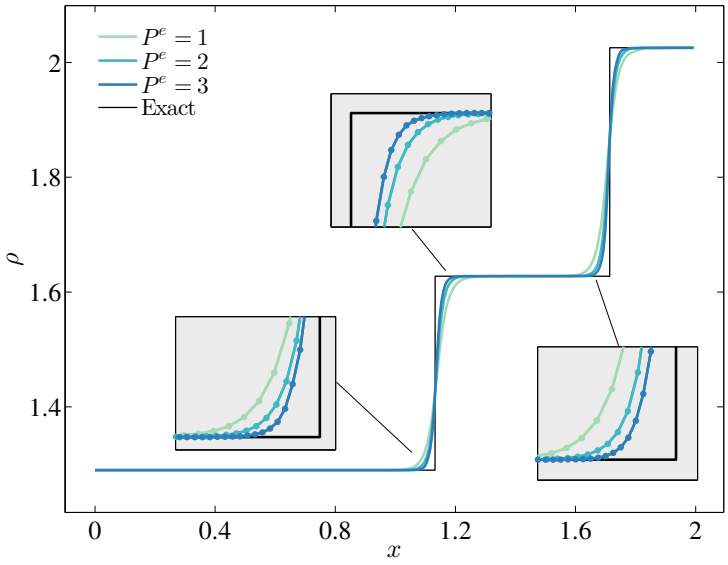

Figure 5. Line plot at $y = 0.2$ of density distribution for the oblique shock reflection problem. The dots represent the average values over control volumes.

IV. Conclusion

The high-order DCVFEM is successfully extended to the solution of the Euler equations in the one- and two-dimensional case. The derivation for the general multi-dimensional case is reported, and the solution to selected test cases is presented. The shock waves and small length scales are accurately approximated, and the numerical solution is free from apparent unphysical oscillations as the polynomial order of accuracy is increased. This desirable feature is related to the weak formulation of the of the DCVFEM, which allows for naturally implement the flux formulation and slope limiting on the control volume's faces at sub-element level.

Acknowledgment

This research is partially supported by Diputación Foral de Bizkaia under Grant BFA/DFB-6/12/TK/-2012/00020, by the Basque Government through the BERC 2014-2017 program and by the Spanish Ministry of Economy and Competitiveness MINECO: BCAM Severo Ochoa accreditation SEV-2013-0323.

Goran Stipcich and Lakhdar Remaki were partially funded by the Project of the Spanish Ministry of Economy and Competitiveness with reference MTM2013-40824-P.

References

[1]Martinez, M. J., "Comparison of Galerkin and control volume finite element for advection-diffusion problems," *International Journal for Numerical Methods in Fluids*, Vol. 50, 2006, pp. 347–376.

[2]Baliga, B. R. and Patankar, S. V., "A new finite-element formulation for convection-diffusion problems," *Numerical Heat Transfer, Part B: Fundamentals*, Vol. 3, No. 4, 1980, pp. 393–409.

[3]Schneider, G. E. and Raw, M. J., "A skewed, positive influence coefficient upwinding procedure for control-volume-based finite-element convection-diffusion computation," *Numerical Heat Transfer, Part B: Fundamentals*, Vol. 9, No. 1, 1986, pp. 1–26.

[4]Masson, C., Saabas, H. J., and Baliga, B. R., "Co-located equal-order control-volume finite element method for two-dimensional axisymmetric incompressible fluid flow," *International Journal for Numerical Methods in Fluids*, Vol. 18, 1994, pp. 1–26.

[5]Saabas, H. J. and Baliga, B. R., "Co-located equal-order control-volume finite-element method for multidimensional, incompressible fluid flow - Part I: formulation," *Numerical Heat Transfer, Part B: Fundamentals*, Vol. 26, No. 4, 1994, pp. 381–407.

[6]Saabas, H. J. and Baliga, B. R., "Co-located equal-order control-volume finite-element method for multidimensional,

incompressible fluid flow - Part II: verification," *Numerical Heat Transfer, Part B: Fundamentals*, Vol. 26, No. 4, 1994, pp. 409–424.

[7]Banaszek, J., "Comparison of control volume and Galerkin finite element methods for diffusion-type problems," *Numerical Heat Transfer, Part B: Fundamentals*, Vol. 16, No. 1, 1989, pp. 59–78.

[8]Ciarlet, P. C., "Discrete maximum principle for finite difference operators," *Aequationes Mathematicae*, Vol. 38, 2000, pp. 1676–1706.

[9]Piller, M. and Stalio, E., "Development of a mixed control volume - Finite element method for the advection-diffusion equation with spectral convergence," *Computers & Fluids*, Vol. 40, No. 1, 2011, pp. 269–279.

[10]Cockburn, B., "Discontinuous Galerkin methods," *Journal of Applied Mathematics and Mechanics*, Vol. 11, 2003, pp. 731–754.

[11]Li, B. Q., *Discontinuous finite elements in fluid dynamics and heat transfer*, Springer-Verlag, Berlin, 2006.

[12]Choi, B. J., Iskandarani, M., Levin, J. C., and Haidvogel, D. B., "A spectral finite volume method for the shallow water equation," *Monthly Weather Review*, Vol. 132, No. 7, 2004, pp. 1777–1791.

[13]Iskandarani, M., Levin, J. C., Choi, B. J., and Haidvogel, D. B., "Comparison of advection schemes for high-order h-p finite element and finite volume methods," *Ocean Modeling*, Vol. 10, 2004, pp. 233–252.

[14]Stipcich, G., Piller, M., Pivetta, M., and Zovatto, L., "Discontinuous control-volume/finite-element method for advection-diffusion problems," *Computers & Fluids*, Vol. 52, No. 1, 2011, pp. 33–49.

[15]Roe, P. L., "Approximate Riemann solvers, parameter vectors, and difference schemes," *Journal of Computational Physics*, Vol. 43, No. 2, 1981, pp. 357–372.

[16]Anderson, J. D., *Computational Fluid Dynamics*, Mc Graw Hill, New York, 1995.

[17]Quarteroni, A. and Valli, A., *Numerical approximation of partial differential equations*, Springer-Verlag, Milano, 1994.

[18]Cockburn, B. and Shu, C. W., "TVB Runge-Kutta local projection discontinuous Galerkin finite element method for scalar conservation laws II: general framework," *Mathematics of Computation*, Vol. 52, 1989, pp. 411–435.

[19]Karniadakis, G. E. and Sherwin, S. J., *Spectral/hp element methods for CFD*, Oxford University Press, Oxford, 2005.

[20]Sod, G. A., "A survey of several finite difference methods for systems on non-linear hyperbolic conservation laws," *Journal of Computational Physics*, Vol. 27, No. 1, 1978, pp. 1–31.

[21]Shu, C. W. and Osher, S., "Efficient implementation of essentially non-oscillatory shock-capturing scheme," *Journal of Computational Physics*, Vol. 77, 1988, pp. 439–471.